catalysts

MDPI

Article

Synthesis of PtNi Alloy Nanoparticles on Graphene-Based Polymer Nanohybrids for Electrocatalytic Oxidation of Methanol

Tung-Yuan Yung [1], Ting-Yu Liu [2,*], Kuan-Syun Wang [2], Che-Chun Liu [2], Shih-Hsuan Wang [2], Po-Tuan Chen [3] and Chi-Yang Chao [4,*]

1 Nuclear Fuels and Materials Division, Institute of Nuclear Energy Research, Lontang, Taoyuan 325, Taiwan; tyyung@iner.gov.tw
2 Department of Materials Engineering, Ming Chi University of Technology, New Taipei City 24301, Taiwan; u01187102@mail2.mcut.edu.tw (K.-S.W.); liu820201@gmail.com (C.-C.L.); u99187003@mail2.mcut.edu.tw (S.-H.W.)
3 Guangzhou Wells Electronic Material Co. Ltd., Guangzhou 510530, China; r92222019@ntu.edu.tw
4 Materials Science and Engineering, National Taiwan University, Taipei 106, Taiwan
* Correspondence: tyliu@mail.mcut.edu.tw (T.-Y.L.); cychao138@ntu.edu.tw (C.-Y.C.); Tel.: +886-2-2908-9899 (ext. 4456) (T.-Y.L.); +886-2-3366-3898 (C.-Y.C.)

Academic Editor: Keith Hohn
Received: 10 September 2016; Accepted: 6 December 2016; Published: 11 December 2016

Abstract: We have successfully produced bimetallic PtNi alloy nanoparticles on poly (diallyldimethylammonium chloride) (PDDA)-modified graphene nanosheets (PtNi/PDDA-G) by the "one-pot" hydrothermal method. The size of PtNi alloy nanoparticles is approximately 2–5 nm. The PDDA-modified graphene nanosheets (PDDA-G) provides an anchored site for metal precursors; hence, the PtNi nanoparticles could be easily bond on the PDDA-G substrate. PtNi alloy nanoparticles (2–5 nm) display a homogenous alloy phase embedded on the PDDA-G substrate, evaluated by Raman, X-ray diffractometer (XRD), thermal gravity analysis (TGA), electron surface chemical analysis (ESCA), and electron energy loss spectroscopy (EELS). The Pt/Ni ratio of PtNi alloy nanoparticles is ~1.7, examined by the energy dispersive spectroscopy (EDS) spectra of transmitting electron microscopy (EDS/TEM spectra) and mapping technique. The methanol electro-oxidation of PtNi/PDDA-G was evaluated by cyclic voltammetry (CV) in 0.5 M of H_2SO_4 and 0.5 M of CH_3OH. Compared to Pt on carbon nanoparticles (Pt/C) and Pt on Graphene (Pt/G), the PtNi/PDDA-G exhibits the optimal electrochemical surface area (ECSA), methanol oxidation reaction (MOR) activity, and durability by chrono amperometry (CA) test, which can be a candidate for MOR in the electro-catalysis of direct methanol fuel cells (DMFC).

Keywords: PtNi alloy nanoparticles; graphene; electrocatalyst; methanol oxidation reaction (MOR); direct methanol fuel cells (DFMC)

1. Introduction

Bimetallic Pt-based nanoparticles with varied metals addition to improve the electrocatalytic durability and anti-carbon monoxide (CO) poisoning ability have been paid attention in recent years, especially in the catalysts of the methanol oxidation reaction (MOR) for the direct methanol fuel cells (DMFC) applications [1–5]. Bimetallic catalysts will be developed to enhance the electrocatalytic properties. PtRu is the most well-known commercial product for DMFC anode electrode usage. Ru removes CO from the Pt active surface [6–8]. In brief, the active site of Pt is the cleavage of the C–H bond, where methanol is attached. The intermediate CO of this process easily forms Pt_x-CO_{add} on the active site during the methanol oxidation process. The oxophilic metals near Pt adsorb CO and oxidize

CO to CO_2 during the reaction. However, Ru atom is easy to be dissolved during the electrocatalytic process. The durability is an important issue for direct methanol fuel cell application (DMFC) [9,10]. Furthermore, the Pt_3Ni bimetallic electrocatalysts on carbon-based substrates have been investigated to catalyze the oxygen reduction reaction (ORR) [11]. Therefore, the addition of transition metal-based catalysts of Ni atom will be considered as a potential alternative owing to their durability and cheaper costs than Ru atom. On the other hand, the enhancement of MOR has been found by carbon-based electrocatalysts, involved the synthesis of electrocatalysts with varied shapes of carbon-based materials supporting, such as C60 nanoparticles, carbon nanotubes, and graphene nanosheets [12–20].

Thus, it is the important issue to combine the bimetallic Pt-based nanoparticles and carbon-based substrates to enhance the electrocatalytic behaviors. Poly(diallyldimethylammonium chloride) (PDDA) has recently been used to form the layer-to-layer structure to modify the graphene surface by non-covalent bonding or π–π interaction [17,18]. Moreover, PDDA immobilized on the carbon nanotubes has been demonstrated [19] to enhance water dispersibility of carbon nanotubes. After immobilized by PDDA, the resulting surface charge of graphene nanosheets is positive charge to prevent the aggregation of graphene nanosheets, and provides an anchored site to homogenously bind the bimetallic Pt-based nanoparticles.

Therefore, the "one-pot" hydrothermal synthesis of PtNi nanoparticles grown on the PDDA-modified graphene (PtNi/PDDA-G) nanohybrids for MOR applications would be investigated in this paper. The morphology of PtNi/PDDA-G nanohybrids would be evaluated by Raman, X-ray diffractometer (XRD), thermal gravity analysis (TGA), electron surface chemical analysis (ESCA), electron energy loss spectroscopy (EELS), and transmitting electron microscopy (TEM) with the energy dispersive spectroscopy (EDS) spectra (EDS/TEM spectra) and mapping technique. Pt on carbon nanoparticles (Pt/C) and Pt on Graphene (Pt/G) nanohybrids would be used as control.

2. Results and Discussion

The in-situ microwave synthesized graphene is examined by XRD, as shown in Figure 1a. The broadened 2θ peak of graphene (002) plane is found at approximately 23°–25°. However, the graphene (002) plane of PtNi/PDDA-G nanohybrids shifted to 20.5°–21°, which shows that the interplanar spacing (d spacing) of graphene is expanded by the intercalation of PDDA, as shown in Figure 1b [21–24]. Furthermore, three XRD peaks is observed at 2θ = 40.2°, 46.3°, and 67.6°, which attributed to the crystalline plane of (111), (200) and (220) planes in the PtNi alloy nanoparticles, respectively [25,26]. These results verified that PtNi alloy nanoparticles can grow on the PDDA-G nanosheets.

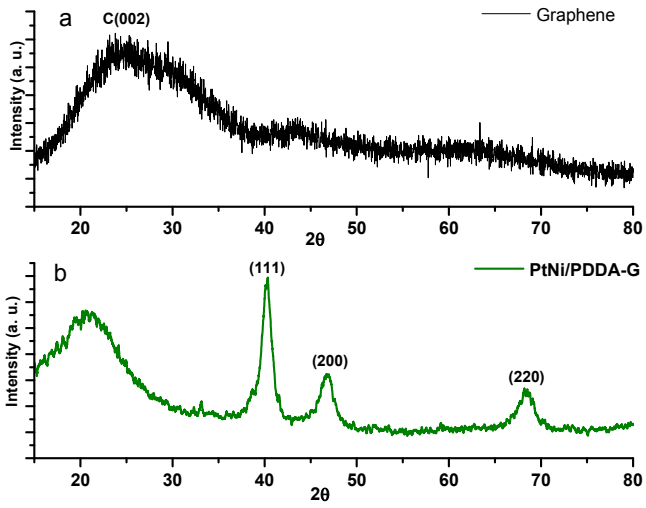

Figure 1. XRD spectra for: (**a**) graphene nanosheets; and (**b**) PtNi/poly(diallyldimethylammonium chloride)-modified graphene nanosheets (PDDA-G) nanohybrids.

Figure 2 shows the Raman spectra of the graphene, PDDA-G and PtNi/PDDA-G. The D and G bands of graphene nanosheets are found at 1350.9 and 1582.1 cm^{-1}, respectively. PDDA-G nanohybrid displays a little bit Raman-shift (D band: 1349.2 cm^{-1} and G band: 1592.4 cm^{-1}), compared with the pristine graphene nanosheets. The D/G band ratios of graphene nanosheets and PDDA-G are 1.4 and 1.7, respectively. It exhibits that graphene nanosheets are reduced and fixed after PDDA addition. However, G and D band peaks cannot be significantly found in the PtNi/PDDA-G, just showed the sharp peak at 582 cm^{-1} (main peaks in the PtNi nanoparticle) and broad background. These results confirm that PtNi nanoparticles truly were deposited on the PDDA-G nanosheets by "one-pot" hydrothermal methods. The absence of G and B band of PtNi/PDDA-G should attribute to PtNi nanoparticles fully embedded on the PDDA-G nanosheets.

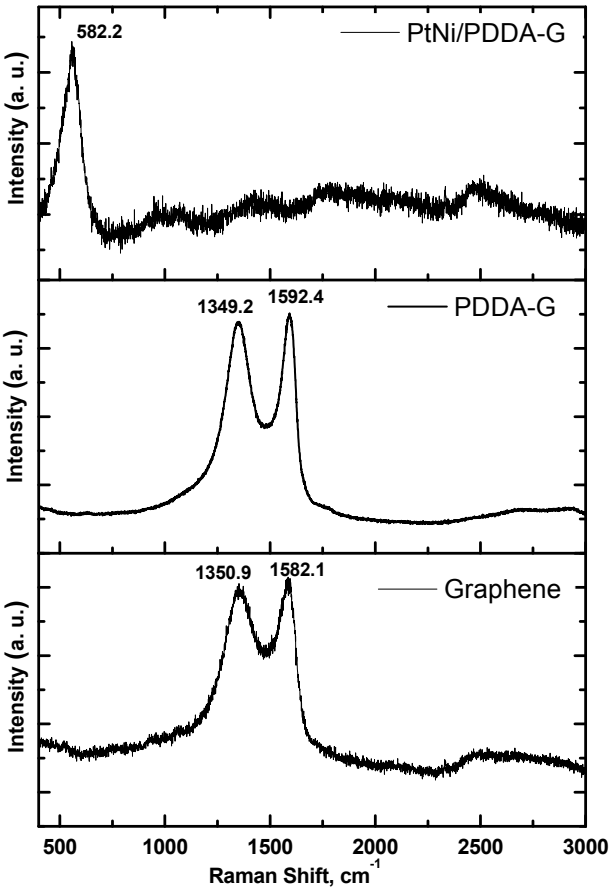

Figure 2. Raman spectra of PtNi/PDDA-G nanohybrids, PDDA-G and graphene nanosheets.

The ESCA analysis of Pt_{4f} and Ni_{2p} in the PtNi/PDDA-G nanohybrids is revealed in Figure 3 and Table 1. The binding energies of the Pt metal phases (Pt^0 phase) were 70.9 eV ($Pt_{4f\text{-}7/2}$) and 74.2 eV ($Pt_{4f\text{-}5/2}$), respectively. Moreover, the Pt^{2+} on phase (PtO and $Pt(OH)_2$) were 71.8 eV ($Pt_{4f\text{-}7/2}$) and 75.3 eV ($Pt_{4f\text{-}5/2}$), which is similar with the literature [24,27–29], as shown in Figure 3a. The ratio of Pt^0/Pt^{2+} was approximately 1.26, which implies that the Pt metal phase is dominant in PtNi/PDDA-G nanocomposites. The Ni_{2p} curve-fitting results show that the estimated Ni metal phase (Ni^0 phase) (855.5 and 873.2 eV) ratio to Ni^{2+} (for $Ni(OH)_2$ and NiOOH) was 1.01, as shown in Figure 3b. By the way, there are two broad satellite peaks (~862 and ~881 eV) in the Ni_{2p} spectrum adjacent to the main peaks, similar with the literature [29]. Furthermore, C_{1s} curve fitting in the PtNi/PDDA-G shows that the two peaks of C=C (284.8 eV) and C–O–C (286.2 eV). O_{1s} curve-fitting results present four functional groups of oxygen, phenol (533.9 eV), C–OH (532.6 eV), C=O (531.6 eV) and C–O–C (530.1 eV), as shown in Table 1. These results confirm again that PtNi nanoparticles anchored on the PDDA-G nanosheets.

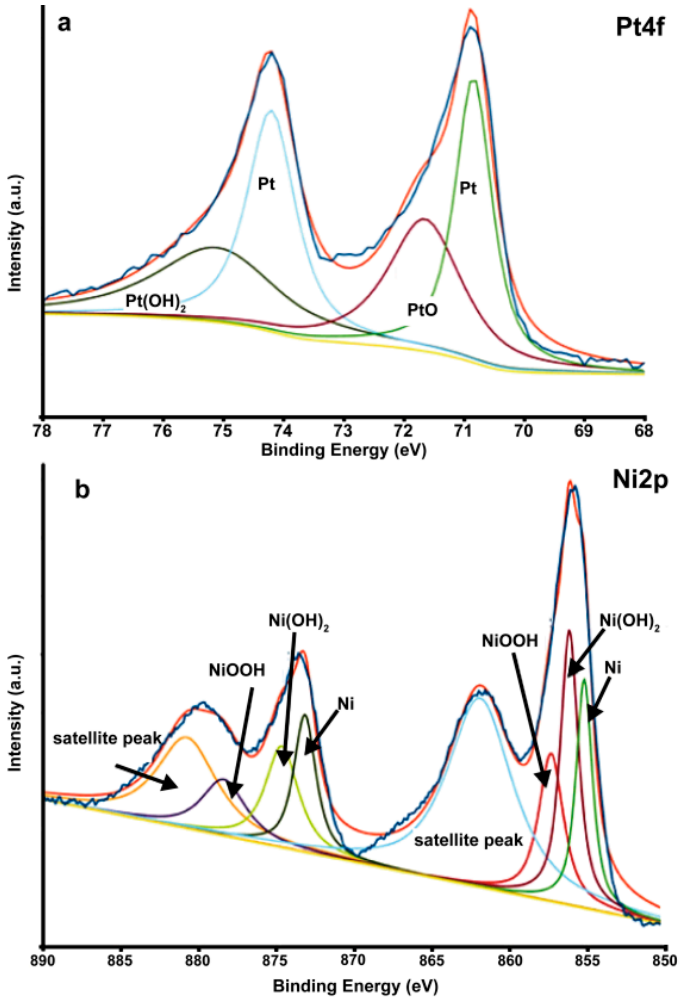

Figure 3. Electron surface chemical analysis (ESCA) spectra of: (**a**) Pt_{4f}; and (**b**) Ni_{2p} in the PtNi/PDDA-G nanohybrids.

Table 1. Fitting peaks of the ECSA spectra of PtNi/PDDA-G nanohybrids.

Atom	Binding Energy (eV)	Peak Area (%)
C_{1s}	284.8	83.81
	286.2	16
O_{1s}	533.9	26.83
	532.6	18.31
	531.6	24.42
	530.1	30.44
N_{1s}	400.5	63.69
	399.4	36.31
Ni_{2p}	879.8	19.36
	874.6	7.86
	873.2	8.06
	861.8	28.08
	856.8	18.17
	855.5	18.47
Pt_{4f}	75.3	19.27
	74.2	25.29
	71.8	24.81
	70.9	30.63

The morphology of PtNi/PDDA-G is examined by high resolution transmission electron microscope (HR-TEM, Figure 4). The result shows that PtNi alloy nanoparticles are approximately 2–5 nm (darker dots) and the size of graphene nanosheets is 100–500 nm in the bottom layer (lighter background), as shown in Figure 4a,b. The selected area electron diffraction (SAED) shows that the diffraction pattern of PtNi alloy nanoparticles [30] displays multi-crystalline structure (Figure 4c), and graphene-based (PDDA-G) nanosheets exhibits the hexagonal lattice structure with ellipse-shaped points (Figure 4d), which proves that PtNi alloy nanoparticles embed on the few layers of PDDA-G nanosheets. Moreover, the HR-TEM image (Figure 4b) shows that the coverage area of PtNi nanoparticles is up to 80%. The shape Raman peak (582.2 cm^{-1}) with broad background come from the PtNi nanoparticles, which is the reason why the G and D band (graphene phases) disappeared in Raman spectra of PtNi/PDDA-G (Figure 2).

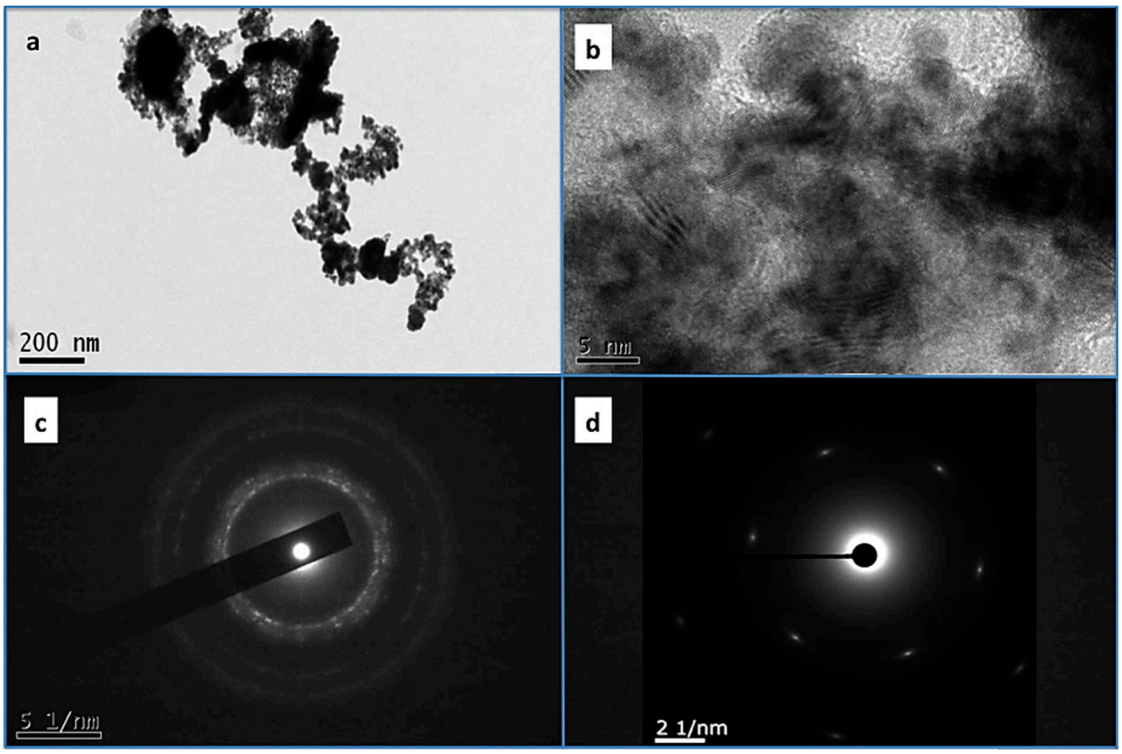

Figure 4. (**a**,**b**) High resolution transmission electron microscope (HR-TEM) images of PtNi/PDDA-G nanohybrids. The selected area electron diffraction (SAED) images of: (**c**) bimetallic PtNi alloy nanoparticles; and (**d**) graphene-based (PDDA-G) nanosheets in the PtNi/PDDA-G nanohybrids.

EDS spectra (Figure 5a), dark-field and mapping images (Figure 5c) from transmission electron microscope (TEM) are applied to differentiate the compositions of PtNi/PDDA-G nanohybrids. Pt/Ni atomic ratio is about 1.61 in the bimetallic PtNi alloy nanoparticles, observed by EDS spectrum (Figure 5a). Dark field TEM image in Figure 5c shows the distribution of the bimetallic PtNi alloy nanoparticles. The location of bright dots is PtNi alloy nanoparticles. Furthermore, PtLα1 (yellow) and NiKα1 (green) mapping displays the Pt and Ni elements are homogenously distributed on the PDDA-G, as shown in Figure 5c.

Thermal gravity analysis (TGA) analysis (Figure 6) shows the loaded weight content (%) of PDDA and PtNi alloy nanoparticles in the PtNi/PDDA-G nanohybrids. The weight loss (%) of PDDA occurs at 270 to 305 °C, and the estimated PDDA content is ~5 wt % covered on the graphene surface. At 305 to 500 °C, graphene nanosheets are decomposed to CO_2. After 500 °C, the residual weight (30.87 wt %) might be the PtNi alloy nanoparticles and carbon residues.

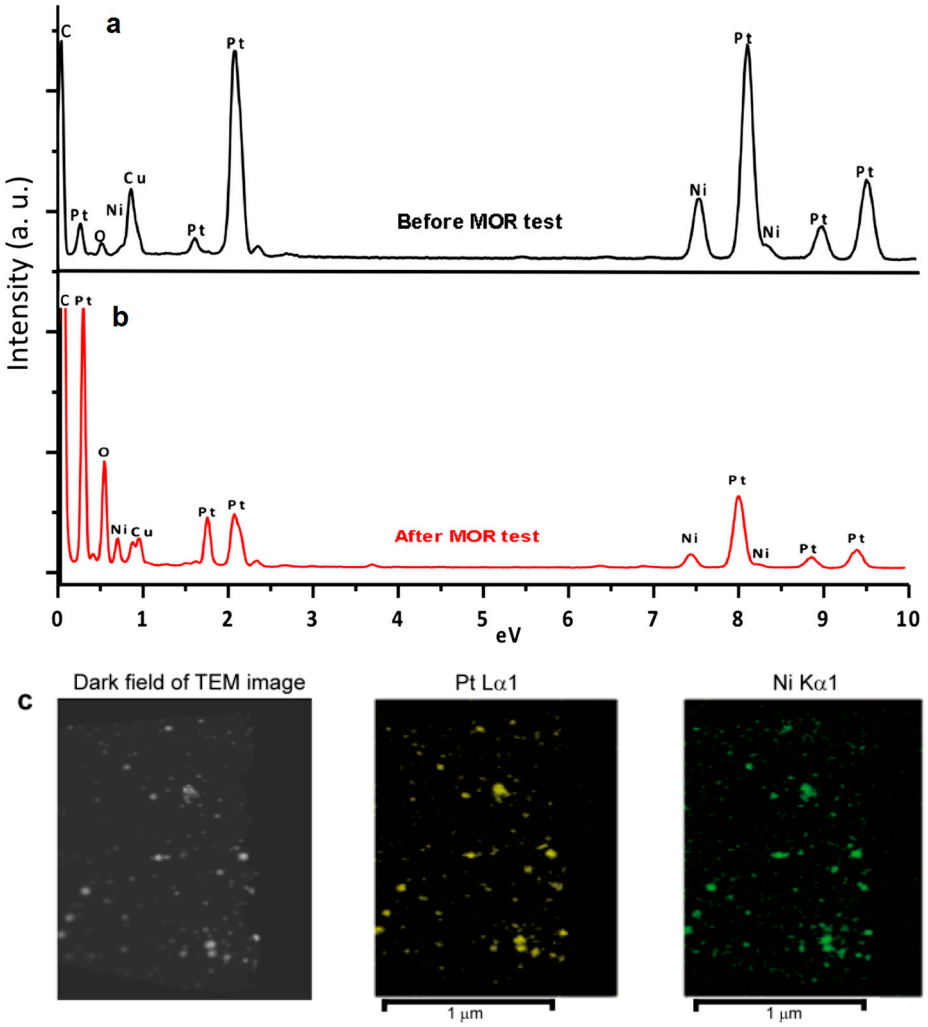

Figure 5. Energy dispersive spectroscopy (EDS)/TEM spectra of PtNi/PDDA-G nanohybrids: (**a**) before; and (**b**) after 300-cycle of MOR tests. (**c**) TEM (Z-contrast) dark-field image and EDS mapping of Pt and Ni before methanol oxidation reaction (MOR) tests.

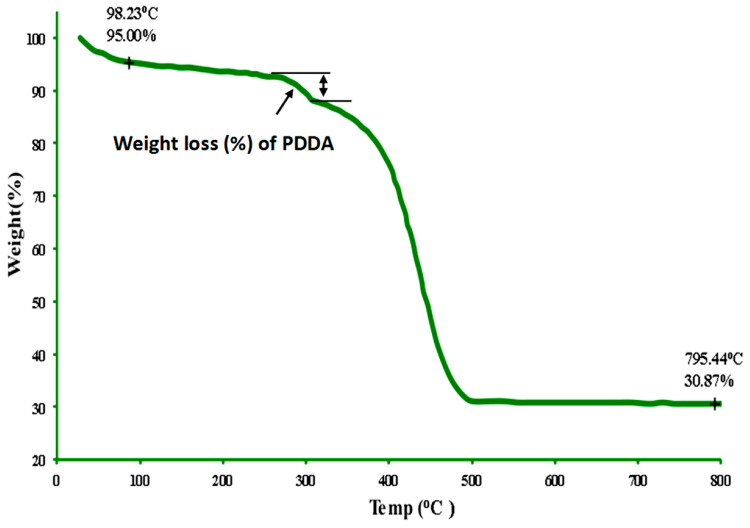

Figure 6. Thermal gravity analysis (TGA) analysis of PtNi/PDDA-G nanohybrids.

The cyclic voltammetry (CV) is examined in the 0.5 M H_2SO_4 aqueous to test the oxidation-reduction reaction ability of PtNi/PDDA-G. Compared with the Ag/AgCl reference electrode, the calculated hydrogen adsorption area of the electrochemical surface area (ECSA) is 40.9 m^2/g of PtNi/PDDA-G, 32.4 m^2/g of Pt/C and 24.16 m^2/g of Pt/G at −0.2 to 0.0 V, as shown in Figure 7a. PtNi/PDDA-G exhibits the highest ECSA, compared with Pt/C and Pt/G.

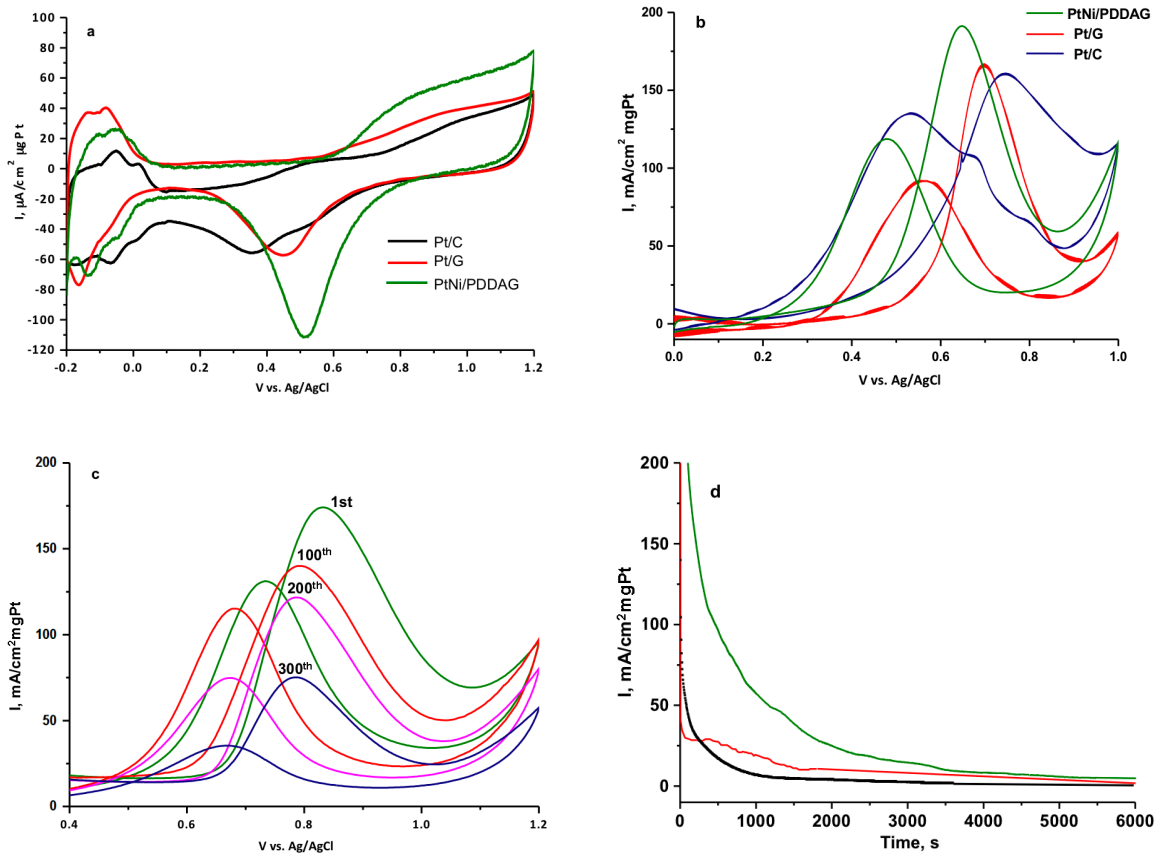

Figure 7. Electrochemical study of PtNi/PDDA-G, Pt/G and Pt/C: (**a**) cyclic voltammetry (CV) curves for PtNi/PDDA-G, Pt/G and Pt/C; (**b**) MOR tests of PtNi/PDDA-G, Pt/G and Pt/C; (**c**) the first, 100th, 200th and 300th cycles of MOR tests in the PtNi/PDDA-G; and (**d**) chrono amperometry (CA) tests at 0.75 V of PtNi/PDDA-G, Pt/G and Pt/C.

Further, the methanol oxidation reaction (MOR) activity of three electrocatalysts (PtNi/PDDA-G, Pt/C and Pt/G) is examined in the 0.5 M H_2SO_4 + 0.5 M CH_3OH aqueous at 0.0 to 1.0 V with a scan rate of 50 mV/s for 1st cycle scanning, as shown in Figure 7b and Table 2. In forward peak (I_f) scanning of PtNi/PDDA-G from 0.0 to 1.0 V, the onset potential is found at 0.41 V, and the apex of I_f was at 0.62 V (287.2 mA/(cm^2·mg)), which is high than Pt/G (161.4 mA/(cm^2·mg)) and Pt/C (158.2 mA/(cm^2·mg)). In backward peak (I_b) scanning of PtNi/PDDA-G from 1.0 to 0.0 V, the onset potential is found at 0.71 V, and the apex of I_b is at 0.47 V (141.3 mA/(cm^2·mg)), which is higher than Pt/G (89.8 mA/(cm^2·mg)) and Pt/C (134.5 mA/(cm^2·mg)). The results demonstrate that PtNi/PDDA-G displays the best MOR activity.

Table 2. Comparison of the electrocatalytic properties of PtNi/PDDA-G, Pt/G and Pt/C nanohybrids.

Electro-Catalysts	ECSA (m^2/g)	I_f (mA/(cm^2·mg))	I_b (mA/(cm^2·mg))	CA (mA/(cm^2·mg))
PtNi/PDDA-G	40.90	287.2	141.3	11.3
Pt/G	24.16	161.4	89.8	5.4
Pt/C	32.40	158.2	134.5	0.3

The area of I_f (1.59×10^{-2} Coulomb (C)) is designated to methanol oxidation, and the area of I_b (8.24×10^{-3} C) is attributed to the amount of Pt-CO_{add} and other oxidants on the activation site of PtNi/PDDA-G [24,30]. The I_f/I_b ratio at 1st scan of PtNi/PDDA-G is 1.93 calculated from the curves in Figure 7b, which indicates that the efficiency of methanol oxidation is more than that of the CO and other oxidants [24,31]. Furthermore, I_f/I_b ratio of PtNi/PDDA-G increased to 2.54 at 300th cycles scanning (Figure 7c). The highest ratio of I_f/I_b at 1st scan is Pt/G (2.49) and the lowest ratio is found at Pt/C (1.37). Although Pt/G displays the best the efficiency of methanol oxidation, the optimal ECSA and MOR activity of the electrocatalyst is PtNi/PDDA-G.

The Chrono amperometry (CA) and 300-cycles of MOR tests are used to evaluate the electrocatalytic durability activity of aforementioned three electrocatalysts. The CA curve of PtNi/PDDA-G gradually decreases with increasing reaction time. After 6000 s of CA measurement at 0.75 V, the current density of PtNi/PDDA-G remains on the order of ~10^{-6} A/cm^2, as shown in Figure 7d. The CA test result shows that PtNi/PDDA-G displays the best durability of electrocatalysts for MOR.

Finally, PtNi/PDDA-G nanohybrids after 300-cycles of MOR tests were examined by EDS/TEM spectra (Figure 5b). The Pt/Ni ratio decreases from 1.70 to 1.18 and the O elements significantly increase, induced to some interactions between methanol and electrocatalysts. Similar results are found at EELS (Figure 8), the metal phase to oxide phase ratios after 300-cycles of MOR tests changes from 1.15 to 0.78 in the Pt_{4f} spectra (Figure 8a,b) and that from 0.81 to 0.33 in the Ni_{2p} spectra (Figure 8c,d), respectively. These results confirm that the metal phase (Pt and Ni) oxidation is executed during MOR.

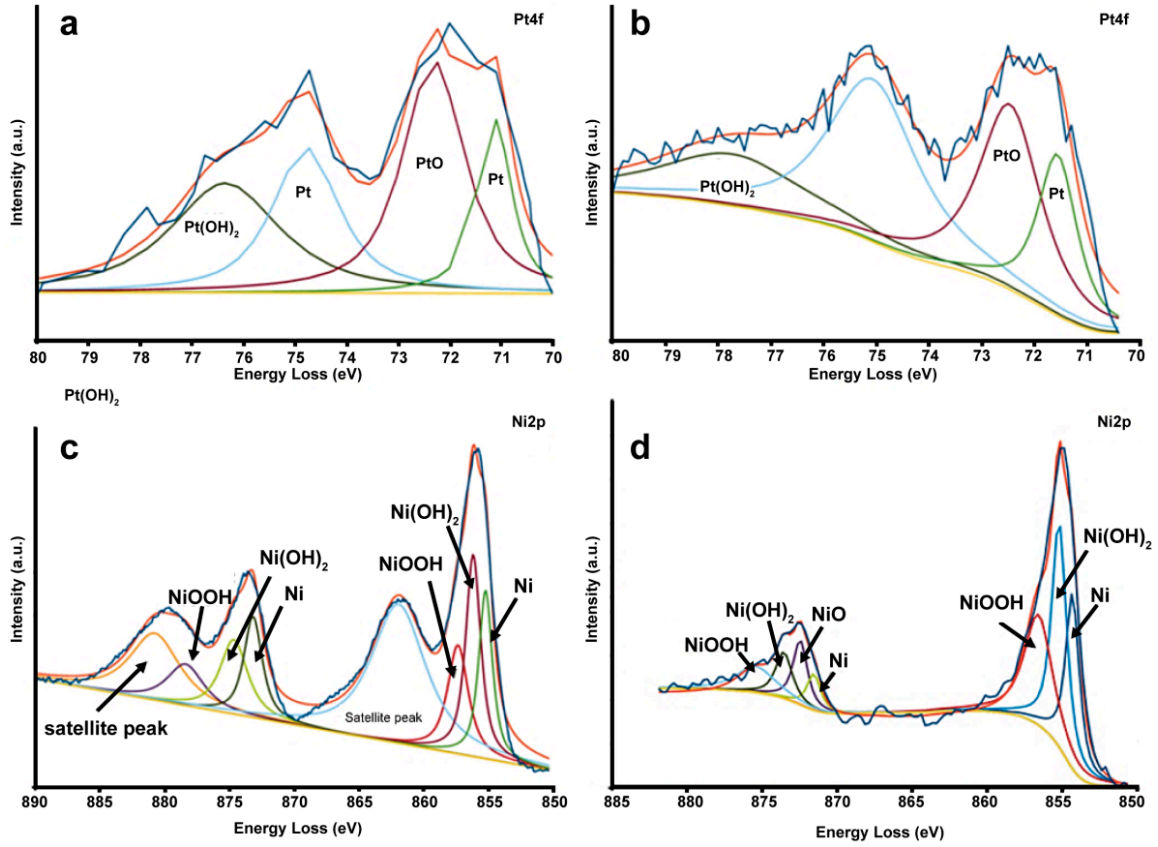

Figure 8. Electron energy loss spectroscopy (EELS) spectra of PtNi/PDDA-G nanohybrids. The electron energy loss (eV) of: (**a**) Pt_{4f}; and (**c**) Ni_{2p} before MOR test; and that of: (**b**) Pt_{4f}; and (**d**) Ni_{2p} after 300-cycles of MOR tests.

3. Materials and Methods

3.1. Fabrication of PtNi Bimetallic Nanoparticle on PDDA-Modified Graphene

The graphene nanosheets were prepared by the direct microwave exfoliated method with the graphite sheets. First, 0.1 g of graphite (Aldrich Co., St. Louis, MO, USA) was put into a 25 mL of round-bottom flask and treated in the microwave synthesis system (CEM Discover Du7046, CEM Coporation, Matthews, NC, USA) with a power output of 20 W at 80 °C for 10 s. Then, 100 mg of the as-prepared graphene nanosheets was added to 50 mL of 3.5 wt % PDDA aqueous (Aldrich, Co., St. Louis, MO, USA) in the 100 mL of flask and then heated at 90 °C for 4 h. The PDDA-modified graphene (PDDA-G) were fabricated. Further, 0.45 mmol of Pt precursors (K_2PtCl_6), 0.45 mmol of Ni precursors ($Ni(NO_3)_2$), hydrazine hydrates, and 2.5 mL of H_2O were added into the aforementioned PDDA-G solution. Then, the mixed solution was transferred into a Teflon-lined autoclave and heated at 90 °C for 24 h, which is as so-called the one-pot hydrothermal method. After washed, centrifuged three times and dried at 90 °C, the PtNi bimetallic nanoparticles embedded on PDDA-G substrates (PtNi/PDDA-G) were prepared. The synthesis of Pt/G nanohybrids can follow our previously method [24], and Pt/C purchased from Union Chemicals, Ltd. (Hong Kong, China).

3.2. Characterizations

The Characterizations of PtNi/PDDA-G nanohybrids were examined with X-ray Diffraction (XRD) using the Bruker D8 diffractometer (Bruker, Berlin, Germany), which was equipped with a Cu Kα X-ray source. Raman analysis was excitation with 532 nm laser and data collection with Horiba Jovin Yvon iHR550 spectrometer (Horiba Instrument Inc., Edison, NJ, USA).

The chemical compositions of PtNi/PDDA-G nanohybrids were examined by ESCA (Thermo VG ESCAlab 250, VG System Ltd., East Grinstead, UK), which was equipped with a dual anode (Mg Kα/Al Kα) X-ray source. ESCA results in this study were collected by Mg Kα X-ray source. The high-resolution micro-structural images of PtNi/PDDA-G were analyzed by TEM (JOEL FEM 2100F, JOEL Ltd., Akishima, Tokyo, Japan), which was equipped with the Oxford energy dispersive X-ray spectroscopy (EDS) and electron energy loss spectroscopy (EELS) for the elements analysis. The thermal gravimetric analysis (TGA) was performed by Perkin Elmer Pyris 1 (Perkin Elmer, Shelton, CT, USA). The heating rate is 10 °C/min from room temperature to 800 °C in an oxygen-purge environment.

The electrochemical study of PtNi/PDDA-G nanohybrids was examined by the AUTOLAB potentiostat/galvanostat PGSTAT30 (Metrohm Autolab B.V., Utrecht, The Netherlands). The reference electrode was Ag/AgCl (BSA, Co., Tokyo, Japan), and the counter electrode was a platinum wire (diameter: 0.5 mm, and length: 10 cm) . The working electrode was a 2.31 μg/cm^2 glass-carbon-deposited PtNi/PDDA-G surface. The cyclic voltammetry (CV) was applied at a scan rate of 50 mV/s. The electrochemical surface area (ECSA) was calculated using Equation (1) in the potential region of −0.2–0.0 V [20].

$$ESCA = \frac{Q}{210 \times g_{pt}} \quad (1)$$

The chrono amperometry (CA) test of PtNi/PDDA-G nanohybrids was examined at 0.75 V during 6000 s for methanol oxidation electrocatalysis current collection.

4. Conclusions

In this study, we have successfully prepared PtNi/PDDA-G nanohybrids by simple and rapid one-pot hydrothermal methods for electrocatalysts applications. By XRD, ESCA and TEM/EDS results, the particle size of bimetallic PtNi alloy nanoparticles is 2–5 nm and the Pt/Ni ratio is ~1.7 with homogenous distribution on the PDDA-G nanosheets. The ECSA of PtNi/PDDA-G nanohybrids is 40.9 m^2/g, as calculated in the CV test in 0.5 M H_2SO_4. Furthermore, the cyclic MOR tests of PtNi/PDDA-G nanohybrids show that the I_f/I_b ratio increases from 1.93 to 2.54 when the MOR cycles

increase from 1st to 300th cycles. Compared to Pt/G and Pt/C, bimetallic PtNi nanoparticles with graphene-based substrate (PDDA-G) demonstrate the optimal electrochemical surface area (ECSA), MOR activity, and durability during MOR tests, which are potential for the usage of the anode electrode catalysts in the direct methanol fuel cell (DMFC).

Acknowledgments: This work was financially supported by the Ministry of Science and Technology of Taiwan MOST 105-2221-E-131-026 and MOST 105-2622-E-131-001-CC2), the Ministry of Education (104B-38-021) and partially supported by the Institute of Nuclear Energy Research and Academia Sinica.

Author Contributions: Tung-Yuan Yung, Ting-Yu Liu and Chi-Yang Chao conceived and designed the experiments. Kuan-Syun Wang, Shih-Hsuan Wang, Che-Chun Liu performed the experiments. Kuan-Syun Wang, and Po-Tuan Chen contributed ideas and material analyses. Tung-Yuan Yung, Ting-Yu Liu and Chi-Yang Chao wrote the manuscript. All authors read and approved the final manuscript.

Conflicts of Interest: The authors declare no competing financial interest.

References

1. Lu, Y.Z.; Chen, W. One-pot synthesis of heterostructured Pt-Ru for catalytic formic acid oxidation. *Chem. Commun.* **2011**, *47*, 2541–2543. [CrossRef] [PubMed]
2. Chen, W.L.; Xu, P.; Chen, S.W. Enhanced electrocatalytic oxidation of formic acid by platinum deposition on ruthenium nanoparticle surfaces. *J. Electroanal. Chem.* **2009**, *631*, 36–42. [CrossRef]
3. Chen, W.; Kim, J.; Sun, S.; Chen, S. Composition effects of FePt alloy nanoparticles on the electro-oxidation of formic acid. *J. Phys. Chem. C* **2007**, *111*, 11303–11310. [CrossRef]
4. Xu, J.B.; Zhao, T.S.; Liang, Z.X. Synthesis of active platinum-silver alloy electrocatalyst toward the formic acid oxidation reaction. *J. Phys. Chem. C* **2008**, *112*, 17362–17367. [CrossRef]
5. Zhang, J.; Yang, H.; Yang, K.; Fang, J.; Zou, Z.; Wang, H.; Bae, I.-T.; Jung, D.Y. Monodisperse Pt_3Fe nanocubes: Synthesis, characterization, self-assembly, and electrocatalytic activity. *Adv. Funct. Mater.* **2010**, *20*, 3727–3733. [CrossRef]
6. Oetjen, H.F.; Schmidt, V.M.; Stimming, U.; Trila, F. Performance data of a proton exchange membrane fuel cell using H_2/CO as fuel gas. *J. Electrochem. Soc.* **1996**, *143*, 3838–3842. [CrossRef]
7. Frelink, T.; Visscher, W.; van Veen, J.A.R. Measurement of the Ru surface content of electrocodeposited PtRu electrodes with the electrochemical quartz crystal microbalance: Implications for methanol and CO electrooxidation. *Langmuir* **1996**, *12*, 3702–3708. [CrossRef]
8. Dinh, H.; Ren, X.; Garzon, F. Electrocatalysis in direct methanol fuel cells: In situ probing of PtRu anode catalyst surfaces. *J. Electroanal. Chem.* **2010**, *491*, 222–233. [CrossRef]
9. Zelenay, P.; Kim, Y.S.; Bashyam, R.; Choi, J.H. Ruthenium crossover in DMFCs operating with different proton conducting membranes. *ECS Trans.* **2006**, *1*, 437–445.
10. Zhao, X.; Yin, M.; Ma, L.; Liang, L.; Liu, C.; Liao, J.; Lu, T.; Xing, W. Recent advances in catalysts for direct methanol fuel cells. *Energy Environ. Sci.* **2011**, *8*, 2736–2753. [CrossRef]
11. Huang, X.; Zhu, E.; Chen, Y.; Li, Y.; Chiu, C.Y.; Xu, Y.; Lin, Z.; Duan, X.; Huang, Y. A facile strategy to Pt_3Ni nanocrystals with highly porous features as an enhanced oxygen reduction reaction catalyst. *Adv. Mater.* **2013**, *25*, 2974–2979. [CrossRef] [PubMed]
12. Li, Y.; Gao, W.; Ci, L.; Wang, C.; Ajayan, P.M. Catalytic performance of Pt nanoparticles on reduced graphene oxide for methanol electro-oxidation. *Carbon* **2010**, *48*, 1124–1130. [CrossRef]
13. Dong, L.F.; Gari, R.R.S.; Li, Z.; Craig, M.M.; Hou, S. Graphene-supported platinum and platinum-ruthenium nanoparticles with high electrocatalystic activity for methanol oxidation. *Carbon* **2010**, *48*, 781–787. [CrossRef]
14. Stein, A.; Wang, Z.; Fierke, M.A. Functionalization of porous carbon materials with designed pore architecture. *Adv. Mater.* **2009**, *21*, 265–293. [CrossRef]
15. Han, K.I.; Leea, J.S.; Parka, S.O.; Leeb, S.W.; Parkb, Y.W. Studies on the anode catalysts of carbon nanotube for DMFC. *Electrochim. Acta* **2004**, *50*, 791–794. [CrossRef]
16. Deivaraj, T.C.; Lee, J.Y. Preparation of carbon-supported PtRu nanoparticles for direct methanol fuel cell applications—A comparative study. *J. Power Source* **2005**, *142*, 43–49. [CrossRef]
17. Liu, W.; Zhang, J.; Li, C.; Tang, L.; Zhang, Z.; Yang, M. A novel composite film derived from cysteic acid and PDDA-functionalized graphene: Enhanced sensing material for electrochemical determination of metronidazole. *Talanta* **2013**, *104*, 204–211. [CrossRef] [PubMed]

18. Wang, S.; Wang, X.; Jiang, S.P. Self-assembly of mixed Pt and Au nanoparticles on PDDA-functionalized graphene as effective electrocatalysts for formic acid oxidation of fuel cells. *Phys. Chem. Chem. Phys.* **2011**, *13*, 6883–6891. [CrossRef] [PubMed]
19. Yang, D.Q.; Rochette, J.F.; Sacher, E. Spectroscopic evidence for π–π interaction between poly(diallyl dimethylammonium) chloride and multiwalled carbon nanotubes. *J. Phys. Chem. B* **2005**, *109*, 4481–4484. [CrossRef] [PubMed]
20. Pozio, A.; De Francesco, M.; Cemmi, A.; Cardellini, F.; Giorgi, L. Comparison of high surface Pt/C catalysts by cyclic voltammetry. *J. Power Sources* **2002**, *105*, 13–19. [CrossRef]
21. Luo, B.M.; Xu, S.; Yan, X. PtNi alloy nanoparticles supported on polyelectrolyte functionalized graphene as elective electrocatalysts for methanol oxidation. *J. Electrochem. Soc.* **2013**, *160*, F262–F268. [CrossRef]
22. Zhang, S.; Shao, Y.; Liao, H.; Liu, J.; Aksay, I.; Yin, G.; Lin, Y. Graphene decorated with PtAu alloy nanoparticles: Facile synthesis and promising application for formic acid oxidation. *Chem. Mater.* **2011**, *23*, 1079–1081. [CrossRef]
23. Yung, T.Y.; Huang, L.Y.; Chan, T.Z.; Wang, K.S.; Liu, T.Y.; Chen, P.C.; Chao, C.Y.; Liu, L.K. Synthesis and characterizations of Ni-NiO nanoaprticles on PDDA-modified graphene for oxygen reduction reaction. *Nanoscale Res. Lett.* **2014**, *9*, 444. [CrossRef] [PubMed]
24. Yung, T.Y.; Lee, J.Y.; Liu, L.K. Nanocomposite for methanol oxidation: Synthesis and characterization of cubic Pt nanoparticles on graphene sheets. *Sci. Technol. Adv. Mater.* **2013**, *14*, 035001. [CrossRef] [PubMed]
25. Hu, Y.; Wu, P.; Yin, Y.; Zhang, H.; Cai, C. Effects of structure, composition and carbon support properties on the electrocatalytic activity of Pt-Ni-graphene nanocatalysts for the methanol oxidation. *Appl. Catal. B* **2012**, *111*, 208–217. [CrossRef]
26. Hu, Y.J.; Wu, P.; Zhang, H.; Cai, C.X. Synthesis of graphene-supported hollow Pt-Ni nanocatalysts for highly active electrocatalysis toward the methanol oxidation reaction. *Electrochim. Acta* **2013**, *85*, 314–321. [CrossRef]
27. Luo, B.M.; Xu, S.; Yan, X.; Xue, Q. Synthesis and electrochemical properties of graphene supported PtNi nanodendrites. *J. Electrochem. Commun.* **2012**, *23*, 72–75. [CrossRef]
28. Liang, G.; He, L.; Arai, M.; Zhao, F. The Pt-enriched PtNi alloy surface and its excellent catalytic performance in hydrolytic hydrogenation of cellulose. *ChemSusChem* **2014**, *7*, 1415–1421. [CrossRef] [PubMed]
29. Deivaraj, T.C.; Chen, W.; Lee, J.Y. Preparation of PtNi nanoparticles for the electrocatalytic oxidation of methanol. *J. Mater. Chem.* **2003**, *13*, 2555–2560. [CrossRef]
30. Gu, J.; Lan, G.X.; Jiang, Y.Y.; Xu, Y.S.; Zhu, W.; Jin, C.H.; Zhang, Y.W. Shaped Pt-Ni nanocrystals with untrathin Pt-enriched shell derived from one-pot hydrothermal synthesis as active electrocatalysts for oxygen reduction. *Nano Res.* **2015**, *8*, 1480–1496. [CrossRef]
31. Masud, J.; Alam, M.T.; Awaludin, Z.; El-Daed, M.S.; Okajima, K.; Ohsaka, K. Electrocatalytic oxidation of methanol at tantalum oxide-modified Pt electrodes. *J. Power Sources* **2012**, *220*, 339–404. [CrossRef]